doi:10.6041/j.issn.1000-1298.2016.04.001

Numerical Simulation of Accelerated Flow on Hydrofoil Cavitation

Shi Weidong Zhang Junjie Zhang Desheng Zhao Ruijie Zhang Lin
(*National Research Center of Pumps*, *Jiangsu University*, *Zhenjiang* 212013, *China*)

Abstract: In order to study the hydrofoil cavitation characteristics in the process of accelerated flow, detached eddy simulation (DES) and homogeneous cavitation model were employed to simulate the unsteady flow around NACA66 model at attack angle of 5.8°. The cavitation number was 0.99 and the corresponding Reynolds number was 8×10^5. The characteristics of cavitation evolution and flow field structure were obtained in the case of two different accelerations (a_1 = 5 m/s^2, a_2 = 2.5 m/s^2). Different numerical simulation results were obtained by studying different accelerations. Cavitation was first born in the leading edge of the hydrofoil, and grew after a period of time and finally separated. Then the cavitation in the leading edge was reduced and the cavitation at the tail of the hydrofoil was increased and backward spread until rupture. Cavitation was first generated at around 0.6 times of total acceleration time and finished a cycle at about 1.12 times of total acceleration time. Oscillation ranges of the lift coefficient became large and the range of the drag coefficient was small with the increase of acceleration. Using small acceleration, the cavitation developed more slowly. The simulation results obtained by DES turbulence model were more close to the experimental values than those obtained by homogeneous cavitation model. The research results can provide reference basis for cavitation characteristics study of hydraulic mechanical startup process.

Key words: hydraulic machinery; hydrofoil cavitation; accelerated flow; detached eddy simulation

0 Introduction

Cavitation is a complex phenomenon of gas-liquid two-phase flow which often develops in the fluid machinery and can easily cause decline in the hydraulic performance, vibration, noise, erosion and other problems. Meanwhile, it is also related to the unsteady problems of two-phase flow and the study of unsteady viscous flow in hydraulic machinery is pervasive. Unsteady flow occurs when the boundary conditions change, for instance, the start-up and stop process of hydraulic rotating machinery. The study on hydrofoil cavitation characteristics, including the process of formation, development and collapse, has been premised for the hydraulic machinery cavitation.

The domestic and foreign researchers have done intensive studies on the two aspects mentioned above. SORIA, et al[1], made experimental measurements of accelerated flow on NACA0015 hydrofoil at attack angle of 30° using the advanced PIV technology. The results validated that different accelerations have an important effect on the shear stress and vertex structure during the start-up process. FREYMUTH[2] obtained images of complex vertex structure by flow visualization to make a parametric study of air flow on NACA0015 hydrofoil with a constant acceleration. HUTTON, et al[3], found that when attached cavitation appears, vertex cavitation which can lead to cavitation clouds occurs in the downstream flow. The unsteady cloud cavitation flow structure of 2D static hydrofoil was studied by KUBOTA, et al[4], and they found that the cavitation cloud which has a vorticity peak in its core is composed of many cavitation bubbles. To solve the problem of numerical simulation of the large separated flow, SPALART, et al[5-6], proposed DES model and analyzed the advantages compared with the LES model. WU, et al[7], used finite volume method to carry numerical simulation for accelerated flow of NACA0015

Received date: 2015-08-18 Accepted date: 2015-09-23
Supported by National Natural Science Foundation of China (Grant No. 51479083), Project Funded by the Priority Academic Program Development of Jiangsu Higher Education Institutions and Key Research and Development Program of Jiangsu (Grant No. BE2015001)
Corresponding author: Shi Weidong, Professor. E-mail: wdshi@ujs.edu.cn. Tel: +86-1305288312.

hydrofoil at large attack angles and obtain details of structure and development of transient flow during and after the acceleration process. To make numerical calculations on the uncompressed and unsteady flow caused by the transient start-up, HAO, et al[8-9], adopted finite volume method which is based on the dynamic mesh and the results reveal the structure and development of unsteady flow around hydrofoil with different accelerations. HUANG, et al[10], studied the application of DES method in the calculation of cavitation flow and found the prediction of cavitation flow around hydrofoil under high Reynolds number is logical, which can simulate the unsteady characteristics of cavity form and the unsteady details of alternate shedding cavities accurately. LI, et al[11], made a comparison of RANS and DES methods in the simulation of the stall properties of hydrofoil and drew the conclusion that DES method is better. HUITENGA, et al[12-13], analyzed the 3D flow field structure and torque transfer of a certain pump and turbine coupling during the start-up process and proposed the method of hydraulic optimization design about the conditions of accelerated flow. LIU, et al[14], studied the transient characteristics of double-suction pump during the start-up with closed valve and found the simulation of all circuit model is closer to the experiment result.

This paper makes a comparison of simulation and experimental results of NACA0015 hydrofoil at large attack angles and verifies the DES method is applicable to the accelerated flow condition. NACA66 hydrofoil is selected as a research object. Finite volume method is used in the numerical calculation of the hydrofoil cavitation under two accelerated flow conditions to obtain the flow structure and development process, and lay a foundation for the design of hydraulic machinery.

1 Numerical simulation and verification

1.1 Turbulent model

To observe and capture the development of various vertexes in the boundary layer during the acceleration process preferably, DES (detached eddy simulation) model is applied to make numerical simulation. DES is a mix turbulent model which combines the LES (large eddy simulation) and RANS (Reynolds averaged Navier-Stokes). It can greatly lower the calculation cost that LES needs and improve the analysis ability for turbulence. Moreover, DES model gives consideration to the low requirements for the grids at the boundary as RANS.

The DES model based on the SST $k-\omega$ is adopted for this paper. The calculation switches from SST $k-\omega$ to LES model when the turbulence length L_t predicted by SST $k-\omega$ is larger than the size of partial grids. And the turbulence length L_t is replaced by the size of partial grids Δ to calculate the dissipation in the k equation

$$\varepsilon=\beta^* k\omega=k^{3/2}/L_t\rightarrow k^{3/2}/(C_{des}\Delta)\quad(C_{des}\Delta<L_t)\tag{1}$$

Therefore, the SST model is corrected as follows.

$$\varepsilon=\beta^* kF_{des}$$

which
$$F_{des}=\max\left(\frac{L_t}{C_{des}\Delta},1\right)\tag{2}$$

where ε—dissipation rate

Δ—maximum local grid spacing

L_t—length scale of turbulence

C_{des}—0.61 β^*—0.09

1.2 Cavitation model

The homogeneous flow model is used, i. e, the multiphase flow in which the velocity fields of gas and liquid are same. The Zwart model based on the Rayleigh-Plesset equation is adopted. The effect of the density of gas core in water on evaporation is considered. The equation to calculate the mass transferred among the cavitation unit volumes is as follows.

$$m=\begin{cases}F_e\dfrac{3r_{nuc}(1-\alpha_v)\rho_v}{R_B}\sqrt{\dfrac{2}{3}\dfrac{p_v-p}{\rho_l}} & (p<p_v)\\ F_c\dfrac{3\alpha_v\rho_v}{R_B}\sqrt{\dfrac{2}{3}\dfrac{p-p_v}{\rho_l}} & (p>p_v)\end{cases}\tag{3}$$

where α_v—gas volume fraction

p_v—vapor pressure, Pa

p—local environment pressure, Pa

ρ_v—water vapor density, kg/m^3

ρ_l—liquid density, kg/m^3

$F_e=50$; $F_c=0.01$; $r_{nuc}=5\times10^{-4}$; $R_B=10^{-6}$ m.

1.3 Verification of DES model

According to the experiment indocument [1], NACA0015 is selected and placed on a plane which is 800 mm long and 200 mm wide. The attack angle is

30° and the chord is 80 mm. The inlet flow is accelerated to 100 mm/s at different accelerations and the corresponding Reynolds number is 8 000. The 2D sketch of the model is in Fig. 1.

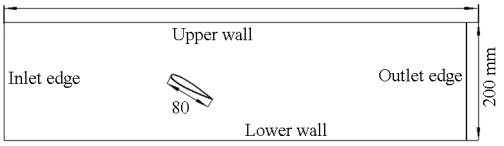

Fig. 1 Sketch of two dimension model

ICEM software is used to divide structured grid. Stretch a layer of grid from the 2D hydrofoil to generate 3D structured grid. The amount of total grids is 400 000. Grids around the hydrofoil are refined and the value of Y^+ is controlled to be 0 ~ 18. Fig. 2a is the velocity field of simulation at one moment after the start-up and the corresponding experimental result is in Fig. 2b. The moment is t/t_a (t means a certain time and t_a means the time of acceleration). The acceleration is $a = 100$ mm/s^2 and Reynolds number is $Re = 8\,000$.

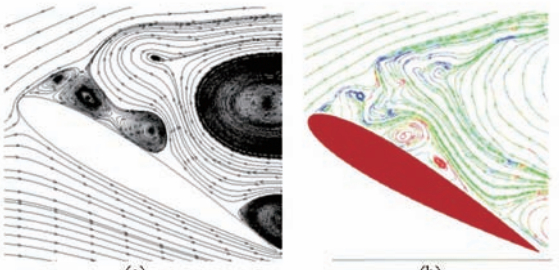

Fig. 2 Comparison of numerical and experimental results

And $t_a = U_\infty / a$ is the time scale of the acceleration process and U_∞ = 100 mm/s is the velocity after accelerating. And t_a is 1s corresponding to accelerated flow whose acceleration is $a = 100$ mm/s^2. The specific acceleration process can be depicted as follows.

$$\begin{cases} v_t = at & \left(t \leqslant \dfrac{100}{a}\right) \\ v_t = 100 & \left(t > \dfrac{100}{a}\right) \end{cases} \tag{4}$$

It can be found from Fig. 2 that the position and development of the vertex in the simulation is in accord with that in experiment. It is verified that the DES model is reliable for the prediction of the characteristics of accelerated flow around hydrofoil.

2 Physical model and boundary conditions

2.1 Physical model

A NACA66 hydrofoil is used to reveal the cavitation development of hydrofoil in accelerated flow. The geometry of this model is in accord with the case in Leroux's experiment[15-16]. The length of chord is 150 mm and wingspan is 192 mm. The nominal angle of attack α in the experiment is $(6.0 \pm 0.2)°$ and it is selected 5.8° in the simulation. The specific model is illustrated in Fig. 3.

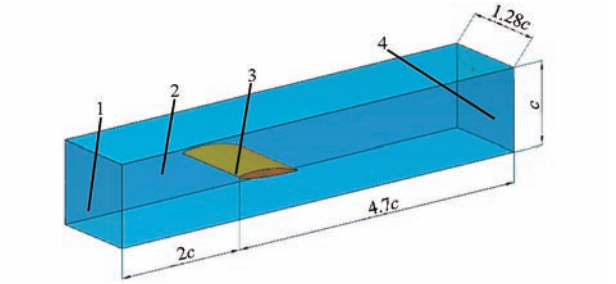

Fig. 3 NACA66(mod) model

ICEM software is used to generate mesh and the type of grid is C. Furthermore, it is 100 × 27 orthogonal grid. It should be noted that the sidewall grid of the hydrofoil must be refined to control the value of Y^+ to be ranged from 0.03 to 6.45. The specific mesh is illustrated in Fig. 4.

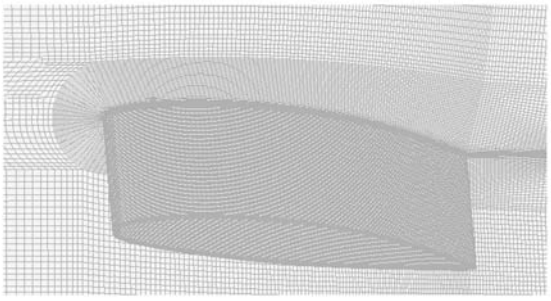

Fig. 4 Grid around hydrofoil

2.2 Boundary conditions

The steady inlet velocity is used as reference velocity $v_{ref} = 5.33$ m/s when setting boundary conditions. The outlet pressure is $p_0 = 17\,636.4$ Pa. Reynolds number is $Re = 8 \times 10^5$ and cavitation number σ is 0.99. The initial velocity is v_0 = 0.33 m/s in the acceleration process. And it is accelerated to $v_{ref} = 5.33$ m/s with different accelerations. Two different accelerations are selected as follows: a_1 = 5 m/s^2, T_{ac1} = 1 s, a_2 = 2.5 m/s^2, T_{ac2} = 2 s. The total computing time is 4 s and time step is 4×10^{-4} s. The specific accelerating process can be depicted as follows.

$$\begin{cases} v_t = 0.33 + at & \left(t \leqslant \dfrac{5}{a}\right) \\ v_t = 5.33 & \left(t > \dfrac{5}{a}\right) \end{cases} \tag{5}$$

3 Simulation results and discussion

3.1 Comparison of simulation and experiment result with constant inlet velocity

To illustrate that the DES turbulent model and Zwart cavitation model are reliable in the simulation of NACA66, the inlet velocity is set as 5.33 m/s and the simulation of cavitation characteristics is at constant inlet velocity. The comparison results of simulation and experiment is as illustrated in Fig. 5. And T means the total acceleration time.

It could be verified that numerical simulation can accurately predict the development of cavitation cloud over acycle. Cavity develops slowly from $T/14$ to $5T/14$. The surface of the sheet cavity is perturbed and part of it fractures, as illustrated in Fig. 5d. And Fig. 5e reveals that the cavity develops into cavity cloud by entrainment which collapses in Fig. 5f. Sheet cavitation restarts to develop around the leading edge after collapse of the secondary cavity for another cycle. Based on the reliability analysis of Fig. 5, then simulate the accelerated flow around hydrofoil. The results of steady cavitation flow with $v_0 = 0.33$ m/s is used as the initial flow field to compute. Meanwhile, considering that 3D computation takes too much time, the 3D model is simplified into 2D. When CFX is used to compute, stretch a layer of grid along the Z axis to analyze the results.

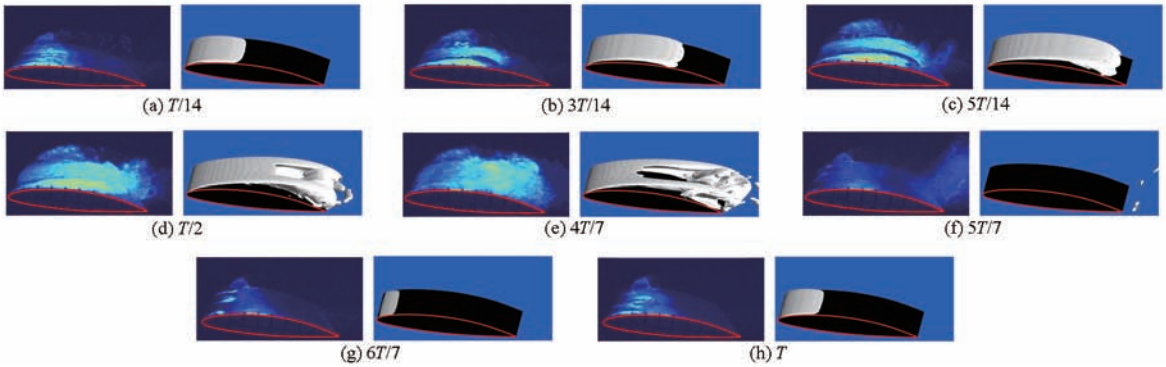

Fig. 5 Comparison of numerical and high speed photography results

3.2 Development of cavitation with different accelerations

Fig. 6 and 7 reveal the development of cavitation within the hydrofoil at different times with different accelerations, including the processes of inception, development, collapse and rebirth. At these two kinds of accelerated flows, cavity firstly appears at the leading edge of hydrofoil and develops after some time. Then it separates at the trailing edge so that the cavity reduces at the leading edge. And cavity at the trailing edge increases and derives aback until collapses. Meanwhile, development of cavitation described above appears repeatedly during the start-up and time interval is very short.

Through further analysis of Fig. 6, during the acceleration process with acceleration $a_1 = 5$ m/s^2, acceleration time $T_{ac1} = 1$ s and total acceleration time $T = 4$ s, cavity firstly appears at $T = 0.66$ s and the first period finishes at $T = 1.14$ s. The process repeats until $T = 4$ s.

As it is illustrated in Fig. 7, during the acceleration process with acceleration $a_2 = 2.5$ m/s^2, acceleration time $T_{ac2} = 2$ s and total acceleration time $T = 4$ s, cavity firstly appears at $T = 1.22$ s and the first period finishes at $T = 2.24$ s. The process repeats until $T = 4$ s.

The time is made dimensionless to discovery

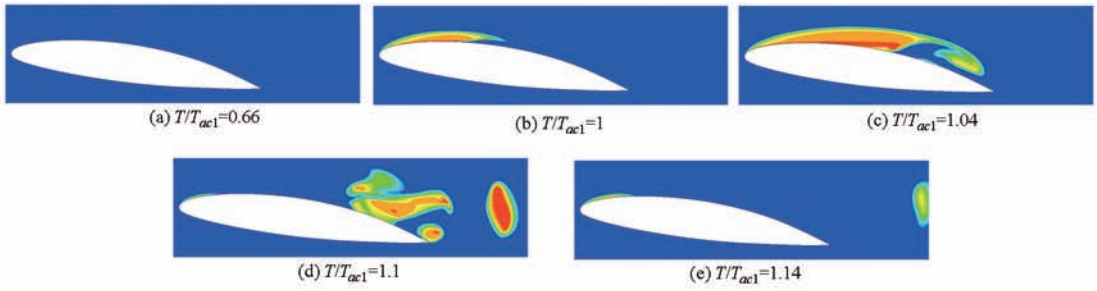

Fig. 6 Cavitation process at different times

characteristics of cavitation development with different start-up accelerations preferably. Through analysis, it can be found that during these two acceleration processes, the cavity firstly appears around $T/T_{ac}=0.6$ and the first cycle finishes around $T/T_{ac}=1.12$.

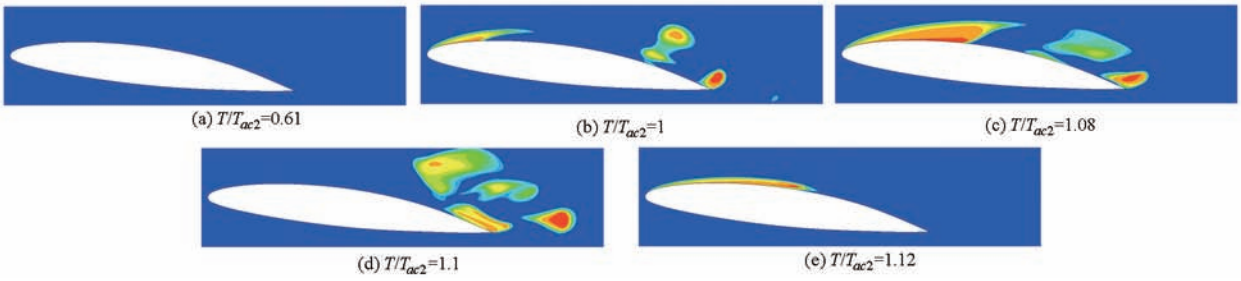

Fig. 7 Cavitation process at different times

3.3 Velocity distribution at different accelerations

Velocity distribution around hydrofoil at different accelerations and moments is given in Fig. 8. It can be found that DES model can effectively simulate the velocity distribution around hydrofoil and change rule of vortices. It is distinct that vortexes around the trailing edge develop more sufficiently by comparison. As is illustrated in Fig. 8, during the initial phase, small vortexes appear at the leading edge because of main flow and back jet flow. However, large clock wise vortexes are generated at the trailing edge under the effect of intense back jet flow. And as time goes on, vortexes around leading edge disappear and enhance at the trailing edge. Meanwhile, the vortexes are driven by main flow to the downstream of hydrofoil until disappear.

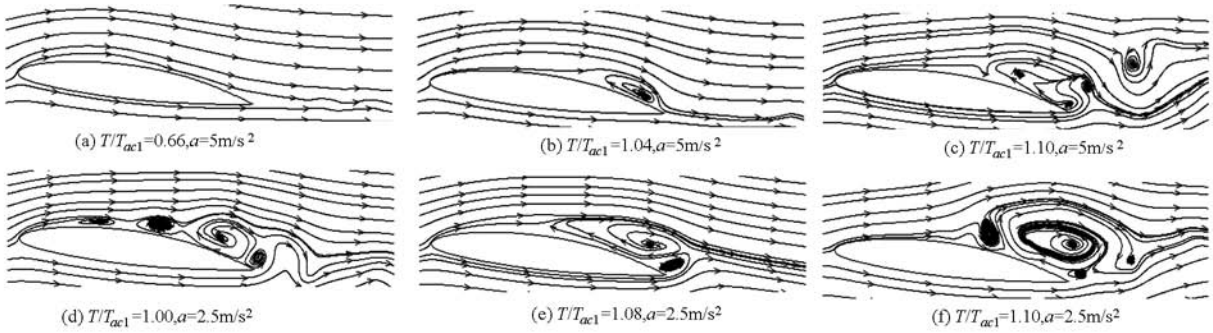

Fig. 8 Velocity field at different times

3.4 Lift and drag characteristics of hydrofoil at different accelerations

It can be found that change tendency of lift coefficient at these two different accelerations is coincident, as is illustrated in Fig. 9. The lift coefficient descends to a small value rapidly and makes a smooth transition to T_{ac}. And it achieves to the maximum around this point. Then the lift coefficient fluctuates periodically. The fluctuation of lift coefficient is ranged from -0.18 to 1.42 for the former accelerated flow and the range is $-0.05 \sim 1.4$ for the latter. The lift fluctuation range is wider with increasing acceleration.

From Fig. 10, it can be found that change tendency of drag coefficient at these two different accelerations is coincident. The drag coefficient descends to a small

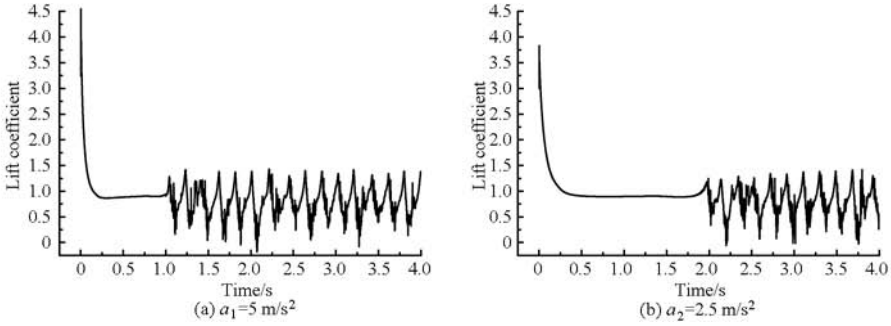

Fig. 9 Lift coefficient at different times

value rapidly and makes a smooth transition to T_{ac}. And it achieves to the maximum around this point. Then the drag coefficient fluctuates periodically. The fluctuation of drag coefficient is ranged from -0.04 to 0.3 for the former accelerated flow and the range is $-0.08 \sim 0.3$ for the latter. The drag fluctuation range is smaller with increasing acceleration.

3.5 Comparison of vapor volume fraction at different accelerations

The total vapor volume fraction on the hydrofoil surface in different accelerated flows and at different moments is as illustrated in Fig. 11. The vapor volume fraction begins to increase when $a_1 = 5\ \text{m/s}^2$, $T = 0.66$ s and achieves to the maximum when $T = 1.08$ s. And the process costs 0.42 s. Then the volume fraction periodically changes irregularly in the future. In addition, the vapor volume fraction begins to increase when $a_2 = 2.5\ \text{m/s}^2$, $T = 1.22$ s and achieves to the maximum when $T = 2.23$ s. And the process costs 1.01 s. By comparison, it can be found that development of the vapor volume fraction from zero to the maximum is slower at lower accelerations and takes more time.

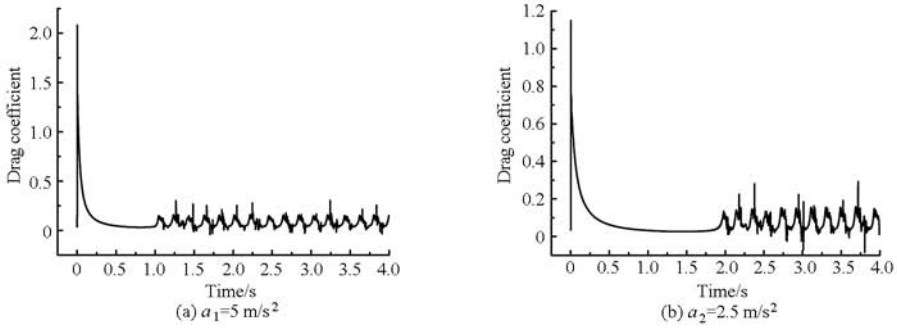

Fig. 10 Lift coefficient at different times

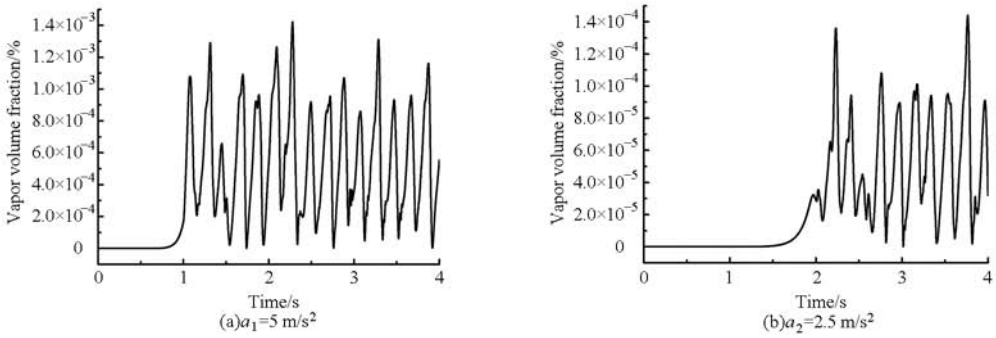

Fig. 11 Vapor volume fraction at different times

4 Conclusion

(1) Through the comparison between simulation and experiment, it is verified that detached eddy simulation and Zwart model can predict hydrofoil cavitation for accelerated flow accurately and provide reference for the study on hydraulic machinery cavitation during start-up.

(2) During start-up, cavity firstly appears at the leading edge of hydrofoil and develops after some time. Then it separates at the trailing edge and reduces at the leading edge. Meanwhile, cavity at the trailing edge increases and derives aback until collapses. The cavity always firstly appears around $T/T_{ac} = 0.6$ and the first cycle finishes around $T/T_{ac} = 1.12$.

(3) The vortexes around the trailing edge develop more sufficiently with decreasing acceleration. Small vortexes at the leading edge are owing to the effects of main flow and back jet flow. But large clockwise vortexes around trailing edge are caused by the intense back jet flow. Meanwhile, as time goes on, vortexes around leading edge disappear and enhance at the trailing edge.

(4) The change tendency of lift and drag coefficients are coincident at different accelerations. The coefficient descends to a small value rapidly and makes a smooth transition to T_{ac}. And it achieves to the maximum around this point. Then the coefficient fluctuates periodically. With the increasing acceleration the lift fluctuation range is wider, while the

drag range is smaller.

(5) Development of the vapor volume fraction from zero to the maximum is slower at lower accelerations and takes more time.

References

[1] SORIA J, NEW H, T, LIM T T, et al. Multigrid CCDPIV measurements of accelerated flow past an airfoil at an angle of attack of 30° [J]. Experimental Thermal and Fluid Science, 2002, 27(5): 667 – 676.

[2] FREYMUTH P. The vortex patterns of dynamic separation: a parametric and comparative study [J]. Progress in Aerospace Sciences, 1985, 22(3): 161 – 208.

[3] HUTTON S P. Studies of cavitation erosion and its relation to cavitating flow patterns [C] // Proceedings of the International Symposium on Cavitation, 1986, 1: 21 – 29.

[4] KUBOTA A, KATO H, YAMAGUCHI H, et al. Unsteady structure measurement of cloud cavitation on a foil section using conditional sampling technique [J]. ASME Journal of Fluids Engineering, 1989, 111(2): 204 – 210.

[5] SPALART P R, JOU W H, STRELETS M, et al. Comments on the feasibility of LES for wings, and on a hybrid RANS/LES approach [C] // LIU C, LIU Z. Advances in DNS/LES, 1st AFOSR International Conference on DNS/LES. Columbus: Greyden Press, 1997: 137 – 148.

[6] FORSYTHE J R, MITCHELL A, HAJEK D. DES and RANS simulations of delta wing vortical flows [M]. Colorado Springs: American Institute of Aeronautics and Astronautics, 2002.

[7] WU Dazhuan, JIAO Lei, WANG Leqin. Numerical simulation of accelerated flow past an airfoil: influence of acceleration [J]. Journal of Engineering Thermophysics, 2006, 27(3): 423 – 425. (in Chinese)

[8] HAO Zongrui, WANG Leqin, WU Dazhuan, et al. Numerical simulation of unsteady flow of impulsively started hydrofoil [J]. Journal of Dalian Maritime University, 2009, 35(2): 131 – 135, 144. (in Chinese)

[9] HAO Zongrui, WANG Leqin, WU Dazhuan. Numerical simulation of unsteady cavitating flow on hydrofoil [J]. Journal of Zhejiang University: Engineering Science, 2010, 44(5): 1043 – 1048. (in Chinese)

[10] HUANG Biao, WANG Guoyu. Application of a SST – DES turbulence model for computation of cavitating flows [J]. China Mechanical Engineering, 2010, 21(1): 85 – 89. (in Chinese)

[11] LI Dong, IGOR Menshov, Yoshiaki Nakamura. Is DES approach better than RANS approach for airfoil stall simulation? [J]. Journal of Northwestern Polytechnical University, 2006, 24(2): 228 – 231. (in Chinese)

[12] HUITENGA H, MITRA N. Improving startup behavior of fluid couplings through modification of runner geometry: part I-fluid flow analysis and proposed improvement [J]. ASME Journal of Fluids Engineering, 2000, 122(4): 683 – 688.

[13] HUITENGA H, MITRA N. Improving startup behavior of fluid couplings through modification of runner geometry: part II-modification of runner geometry and its effects on the operation characteristics [J]. ASME Journal of Fluids Engineering, 2000, 122(4): 689 – 693.

[14] LIU Zhuqing, ZHU Qiang, YANG Wei, et al. Transient characteristics of double-suction centrifugal pump during starting period under shut-off condition [J]. Transactions of the Chinese Society for Agricultural Machinery, 2015, 46(10): 44 – 48, 55. (in Chinese)

[15] LEROUX J B, COUTIER-DELGOSHA O, ASTOLFI J A. A joint experimental and numerical study of mechanisms associated to instability of partial cavitation on two-dimensional hydrofoil [J]. Physics of Fluids, 2005, 17(5): 052101.

[16] LEROUX J B, ASTOLFI J A, BILLARD J Y. An experimental study of unsteady partial cavitation [J]. ASME Journal of Fluids Engineering, 2004, 126(1): 94 – 101.

[17] ZWART P J, GERBER A G, BELAMRI T. A two-phase flow model for predicting cavitation dynamics [C] // Fifth International Conference on Multiphase Flow, Yokohama, Japan, 2004: 152.

[18] HUANG B, WANG G, ZHAO Y, et al. Physical and numerical investigation on transient cavitating flows [J]. Science China Technological Sciences, 2013, 56(9): 2207 – 2218.

[19] HUANG B, YOUNG Y L, WANG G, et al. Combined experimental and computational investigation of unsteady structure of sheet/cloud cavitation [J]. Journal of Fluids Engineering, 2013, 135(7): 071301.

[20] HUANG B, ZHAO Y, WANG G. Large eddy simulation of turbulent vortex-cavitation interactions in transient sheet/cloud cavitating flows [J]. Computers & Fluids, 2014, 92: 113 – 124.

doi:10.6041/j.issn.1000-1298.2016.04.001

绕水翼加速流空化特性数值模拟

施卫东　张俊杰　张德胜　赵睿杰　张　琳
(江苏大学国家水泵及系统工程技术研究中心,镇江 212013)

摘要:为了解翼型加速流动过程中空化特性,采用分离涡湍流模型(Detached eddy simulation, DES)和均相流空化模型对攻角为 5.8°的 NACA66(mod)水翼进行数值模拟,分析了空化数为 0.99、对应雷诺数为 8×10^5 时绕二维水翼的非定常流动。通过模拟 2 种不同加速度(5 m/s^2 和 2.5 m/s^2)情况下空化演变过程和流场结构变化特征,得出了加速过程特有的变化规律:不同加速流下空泡都先在翼型的前缘产生,经过一段时间发展壮大,在翼型尾翼处分离,前缘处空泡减少,尾翼处空泡增加并向后衍生,直至破裂。空化产生于总加速时间的 0.6 倍左右,在总加速时间的 1.12 倍左右结束第一个周期。加速度越小,升力系数振荡范围越小,阻力系数振荡范围越大,空化发展过程越缓慢。

关键词:水力机械;水翼空化;加速流;分离涡模型
中图分类号:V211.1　　**文献标识码**:A　　**文章编号**:1000-1298(2016)04-0001-07

Numerical Simulation of Accelerated Flow on Hydrofoil Cavitation

Shi Weidong　Zhang Junjie　Zhang Desheng　Zhao Ruijie　Zhang Lin
(*National Research Center of Pumps*, *Jiangsu University*, *Zhenjiang* 212013, *China*)

Abstract: In order to study the hydrofoil cavitation characteristics in the process of accelerated flow, detached eddy simulation (DES) and homogeneous cavitation model were employed to simulate the unsteady flow around NACA66 model at attack angle of 5.8°. The cavitation number was 0.99 and the corresponding Reynolds number was 8×10^5. The characteristics of cavitation evolution and flow field structure were obtained in the case of two different accelerations ($a_1=5$ m/s^2, $a_2=2.5$ m/s^2). Different numerical simulation results were obtained by studying different accelerations. Cavitation was first born in the leading edge of the hydrofoil, and grew after a period of time and finally separated. Then the cavitation in the leading edge was reduced and the cavitation at the tail of the hydrofoil was increased and backward spread until rupture. Cavitation was first generated at around 0.6 times of total acceleration time and finished a cycle at about 1.12 times of total acceleration time. Oscillation ranges of the lift coefficient became large and the range of the drag coefficient was small with the increase of acceleration. Using small acceleration, the cavitation developed more slowly. The simulation results obtained by DES turbulence model were more close to the experimental values than those obtained by homogeneous cavitation model. The research results can provide reference basis for cavitation characteristics study of hydraulic mechanical startup process.

Key words: hydraulic machinery; hydrofoil cavitation; accelerated flow; detached eddy simulation

引言

空化是一种气-液两相的复杂流动现象,经常发生于各种流体机械中,容易导致水力性能下降、振动、噪声和空化侵蚀等问题。同时又涉及两相之间流动的非定常问题,而非定常粘性流动在水力机械

收稿日期:2015-08-18　修回日期:2015-09-23
基金项目:国家自然科学基金项目(51479083)、江苏高校优势学科建设工程项目和江苏省重点研发计划项目(BE2015001)
作者简介:施卫东(1964—),男,研究员,博士生导师,主要从事流体机械与工程研究,E-mail:wdshi@ujs.edu.cn

的研究中普遍存在。当边界随时间改变发生变动时,都会引起非定常流动,典型情况如水力旋转机械的启动和停机过程。绕水翼空化特性的研究已经成为各种水力机械空化特性研究的前提,包括空化的形成、发展和溃灭过程。

国内外学者对上述 2 个方面进行了深入研究,SORIA 等[1]采用最新 PIV 技术对绕 NACA0015 翼型 30°攻角加速流动进行了实验测量,验证了不同加速度对启动过程剪切层强度、涡结构的发展有着重要影响。FREYMUTH[2]采用流动显示技术提供了复杂涡结构图像,对以固定加速度加速流过 NACA0015 翼型的空气流动进行了参数化研究。HUTTON 等[3]发现,随着附着空化的产生,下游出现旋涡空化,旋涡空化将产生空化云。KUBOTA 等[4]实验研究了二维静止翼型非定常云型空化流场结构,发现空化云是由许多小的空化气泡组成的,它的中心存在着涡量极值。SPALART 等[5-6]针对大分离流动的数值模拟问题,提出了 DES 模型,分析了区别于 LES 模型的优势。吴大转等[7]采用有限体积法对大攻角 NACA0015 翼型的加速流动进行了数值模拟,给出了加速过程和完成加速后的详细瞬态流动结构和演化过程。郝宗睿等[8-9]采用基于动网格方法的有限体积法对翼型瞬态启动引起的二维不可压缩非定常流动进行了数值计算,计算了不同启动加速度下绕翼型非定常流动的结构及其演化过程。黄彪等[10]研究了 DES 方法在空化流动计算中的应用,发现高雷诺数的绕水翼空化流动的预测是合理的,可以准确地模拟出空穴形态的非定常特性和空泡团交替脱落的非定常细节。李栋等[11]对比了 RANS 方法和 DES 方法在模拟翼型失速特性的能力,得出了 DES 方法对大分离流动体现更强能力。HUITENGA 等[12-13]分析了某水泵和透平耦合的启动过程中三维流场结构和转矩传递,提出了针对加速流工况的水力设计优化思路。刘竹青等[14]对双吸离心泵关阀启动过程的瞬态特性进行了深入研究,得出全回路模型模拟与实验值更接近。

本文采用 NACA0015 大攻角翼型模拟结果与实验结果进行对比,验证 DES 方法对加速流工况流动问题的适用性。然后选取 NACA66 翼型为研究对象,运用有限体积法对 2 种加速流工况水翼的空化特性进行数值计算,以得出不同加速流非定常空化的流动结构和演化过程,为后续水力机械的研究打下基础。

1 数值模拟方法及其验证

1.1 湍流模型

为了更好地观察和捕捉水翼加速流过程中边界各种涡的发展过程,采用分离涡模型(Detached eddy simulation, DES)进行数值模拟。它是结合了大涡模拟(Large eddy simulation, LES)和雷诺时均(Reynolds averaged Navier - Stokes, RANS)模型的混合湍流模型,能够很好地降低大涡模拟所需要的计算成本,提高对湍流解析的能力,兼顾雷诺时均模型对边界层网格的低要求。

采用基于 SST $k-\omega$ 的 DES 模型。当 SST $k-\omega$ 预测的湍流长度 L_t 比局部网格尺寸大时,从 SST $k-\omega$ 模式切换到 LES 模式进行计算。此时,局部网格尺寸 Δ 代替湍流尺度 L_t,用来计算 k 方程中的耗散率,即

$$\varepsilon=\beta^* k\omega=k^{3/2}/L_t\rightarrow k^{3/2}/(C_{des}\Delta)\quad(C_{des}\Delta<L_t)\tag{1}$$

式中 ε——耗散率 Δ——最大局部网格间距

L_t——湍流长度尺度

C_{des}——DES 方程中的标定常数,设定为 0.61

β^*——常数,设定为 0.09

k——湍动能 ω——湍流特征频率

所以,SST 模型在 DES 中被修正为

$$\varepsilon=\beta^* kF_{des}\tag{2}$$

其中

$$F_{des}=\max\left(\frac{L_t}{C_{des}\Delta},1\right)$$

1.2 空化模型

采用均相流模型,即假设气液两相流具有相同速度场的多相流模型。空化模型采用基于 Rayleigh - Plesset 方程的 Zwart 模型。同时考虑水中气核密度对蒸发的影响,空化的单位体积相间质量传输率计算式为

$$m=\begin{cases}F_e\dfrac{3r_{nuc}(1-\alpha_v)\rho_v}{R_B}\sqrt{\dfrac{2}{3}\dfrac{p_v-p}{\rho_l}} & (p<p_v)\\ F_c\dfrac{3\alpha_v\rho_v}{R_B}\sqrt{\dfrac{2}{3}\dfrac{p-p_v}{\rho_l}} & (p>p_v)\end{cases}\tag{3}$$

式中 α_v——气相体积分数

p_v——气化压力,Pa

p——当地环境压力,Pa

ρ_v——气化压力下的水蒸气密度,kg/m^3

ρ_l——液体密度,kg/m^3

式中经验常数分别为:蒸发系数 $F_e=50$;凝结系数 $F_c=0.01$;气核的体积分数 $r_{nuc}=5\times10^{-4}$;空泡半径 $R_B=10^{-6}$ m。

1.3 DES 模型验证

根据文献[1]中的实验,选取 NACA0015 模型,将其放置于一个长 800 mm、宽 200 mm 的二维平面

中，翼型攻角为 30°，弦长为 80 mm，进口加速流从零以不同加速度加速到 100 mm/s，对应的雷诺数为 8 000，该模型的二维示意图如图 1 所示。

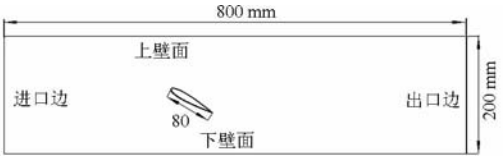

图 1　二维模型示意图

Fig. 1　Sketch of two dimension model

使用前处理 ICEM 软件进行结构化网格划分，将二维翼型往外拉伸一层网格，变成三维结构化网格，总体网格数为 40 万，并对翼型外围进行了加密处理，最后 Y^+ 值控制在 0 ~ 18（Y^+ 表示第 1 层网格中心到壁面的无量纲距离）。如图 2a 所示为启动完成后的某一时刻速度场的模拟结果，并与图 2b 的实验进行了比较。该时刻为 $t/t_a = 3.2$（t 表示某一时刻，t_a 表示加速时间），加速度 $a = 100\ \text{mm/s}^2$，雷诺数 $Re = 8\,000$。其中 $t_a = U_\infty / a$ 为加速过程的时间尺度，U_∞ 为完成加速后的速度，即 100 mm/s。对应 $a = 100\ \text{mm/s}^2$ 加速流动，t_a 为 1 s。具体加速过程可描述为

$$\begin{cases} v_t = at & \left(t \leqslant \dfrac{100}{a}\right) \\ v_t = 100 & \left(t > \dfrac{100}{a}\right) \end{cases} \tag{4}$$

式中　v_t——不同时刻速度，m/s

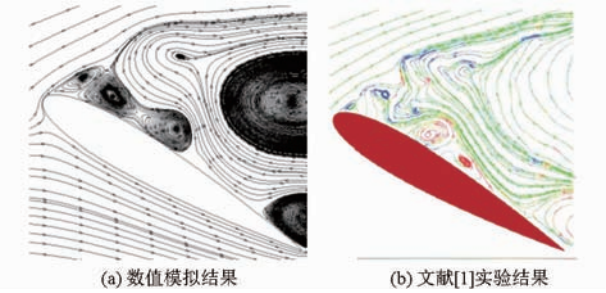

图 2　计算结果与实验结果比较

Fig. 2　Comparison of numerical and experimental results

通过对比可以发现，模拟结果中出现的旋涡所处的位置和涡的发展过程以及结构都与实验结果相互吻合。验证了 DES 模型对预测加速流下绕水翼流动特性的可靠性。

2　物理模型及边界条件

2.1　物理模型

为了说明水翼在加速过程中空化的发展情况，选取 NACA66（mod）模型，几何尺寸与文献[15 - 16]实验的原型情况一致，弦长 150 mm，翼展 192 mm，实验的名义攻角为 $\alpha = (6.0 \pm 0.2)°$，模拟时的攻角为 $\alpha = 5.8°$。具体模型如图 3 所示。

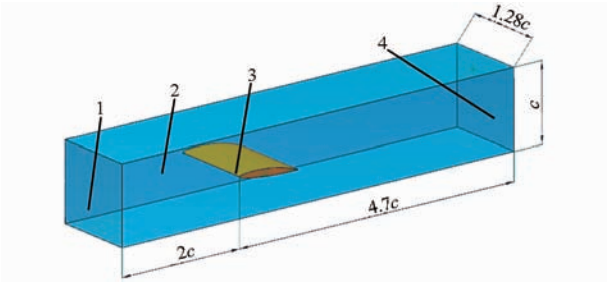

图 3　NACA66（mod）模型

Fig. 3　NACA66（mod）model

1. 速度进口　2. 壁面　3. 翼型　4. 压力出口

采用 ICEM 软件进行网格划分，水翼网格采用 C 型网格，具体为 100 × 27 正交网格，特别注意翼型边壁要进行网格加密，以控制 Y^+ 值在 0.03 ~ 6.45 之间。具体网格如图 4 所示。

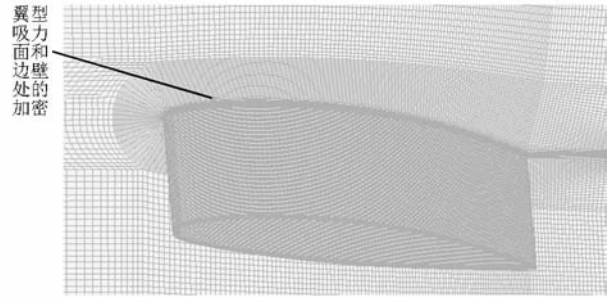

图 4　水翼周围的网格图

Fig. 4　Grid around hydrofoil

2.2　边界条件

边界条件设置时，将稳定后进口速度作为参考速度 $v_{ref} = 5.33\ \text{m/s}$，出口绝对压力 $p_0 = 17\,636.4\ \text{Pa}$。基于翼型弦长 c 计算的雷诺数 $Re = 8 \times 10^5$，空化数 $\sigma = 0.99$。加速过程初始速度 $v_0 = 0.33\ \text{m/s}$，经不同加速度加速到 $v_{ref} = 5.33\ \text{m/s}$。选取 2 种不同加速度 $a_1 = 5\ \text{m/s}^2$，加速时间 $T_{ac1} = 1\ \text{s}$，$a_2 = 2.5\ \text{m/s}^2$，$T_{ac2} = 2\ \text{s}$，总计算时长为 4 s，计算时间步长 Δt 为 4×10^{-4} s，具体加速过程可以描述为

$$\begin{cases} v_t = 0.33 + at & \left(t \leqslant \dfrac{5}{a}\right) \\ v_t = 5.33 & \left(t > \dfrac{5}{a}\right) \end{cases} \tag{5}$$

3　数值模拟结果与讨论

3.1　进口恒定流速下模拟与实验对比

为了更好地说明 DES 湍流模型和 Zwart 空化模型在模拟 NACA66 时的可靠性，首先将进口流速设定为 5.33 m/s，进行恒定流速下空化特性模拟，与文献[15]中的实验结果进行对比，结果如图 5 所示，图中 T 表示加速总时间。

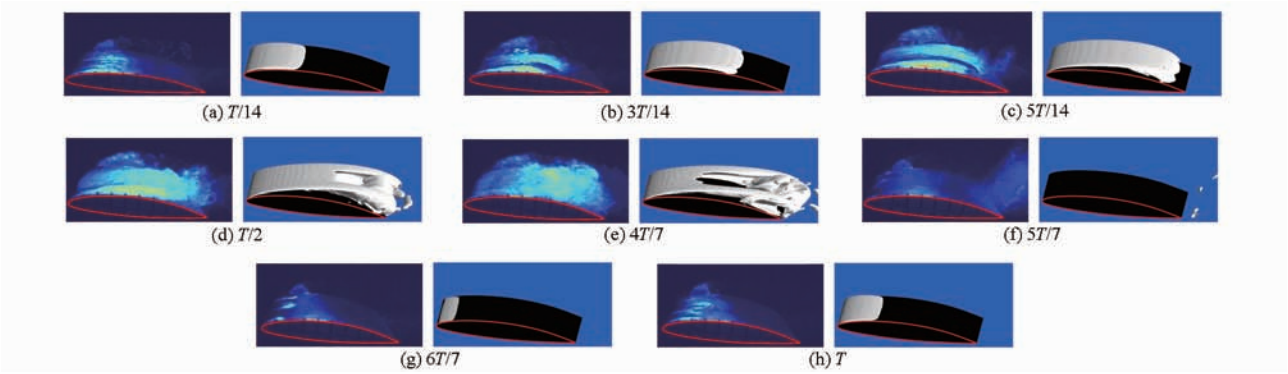

图 5 数值模拟空化图像和高速摄影的对比

Fig. 5 Comparisons of numerical and high speed photography results

上述对比可以说明数值模拟较好地预测了空泡云在周期内的演化过程。空穴在 $T/14 \sim 5T/14$ 中缓慢生长;在图 5d 中,片状空穴表面受到扰动,片状空穴部分断裂;如图 5e 所示,空穴继续向下游卷吸形成空泡团;空泡团在图 5 f 中溃灭;二次空泡溃灭后,在图 5g、5h 中片状空化在翼型头部重新开始生长,开始一个新的周期。

基于上述图 5 中结果可靠性分析,进而模拟翼型加速流工况特性。为了反映空化流动的基本特征,将 $v_0 = 0.33$ m/s 稳态空化流动的结果作为初始流场进行计算。同时考虑到三维计算需要的时间过长,故将三维模型简化为二维,再用 CFX 计算时沿着 Z 轴拉伸一层网格,进行结果分析。

3.2 不同加速度下空化发展过程

图 6、图 7 分别为不同加速流下不同时刻翼型内部空化发展情况,经历了空化初生、发展、溃灭、重生过程。在 2 种加速流下,空泡首先在翼型的前缘产生,经过一段时间后发展壮大,然后在翼型尾翼处分离,前缘处空泡减少,尾翼处空泡增加并向后衍生,直至破裂。同时上述空化发展过程在启动过程中反复呈现,时间间隔很短暂。

具体分析图 6 可知,在加速度 $a_1 = 5$ m/s^2,加速时间为 $T_{ac1} = 1$ s,总时间为 4 s 的加速过程中,空泡首先在 $T = 0.66$ s 时产生,$T = 1.14$ s 后第 1 个周期结束,直到 $T = 4$ s 一直重复上述过程。

从图 7 可知,在加速度 $a_2 = 2.5$ m/s^2,加速时间为 $T_{ac2} = 2$ s,总时间为 4 s 的加速过程中,空泡首先在 $T = 1.22$ s 时产生,$T = 2.24$ s 后第 1 个周期结束,直到 $T = 4$ s 一直重复上述过程。

图中为了更好地找出不同启动加速度下空化发展特征,将时间无量纲化。通过分析可以发现,在 2 种加速流过程中空化都首先产生于 $T/T_{ac} = 0.6$ 左

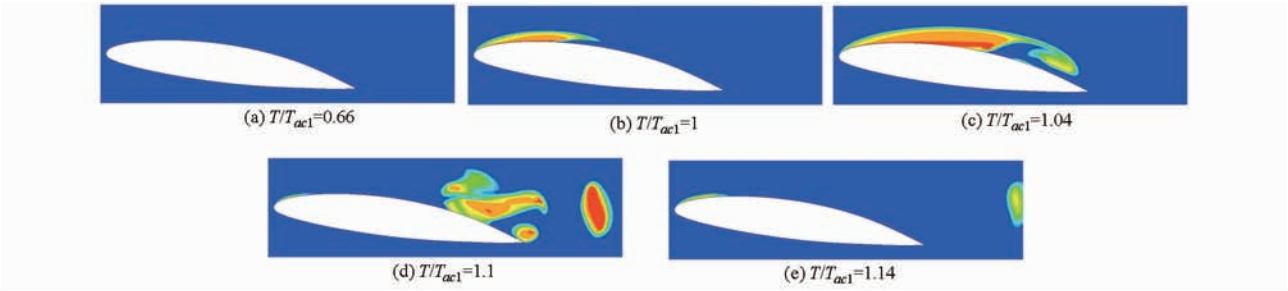

图 6 不同时刻空化发展过程($a_1 = 5$ m/s^2)

Fig. 6 Cavitation process at different times

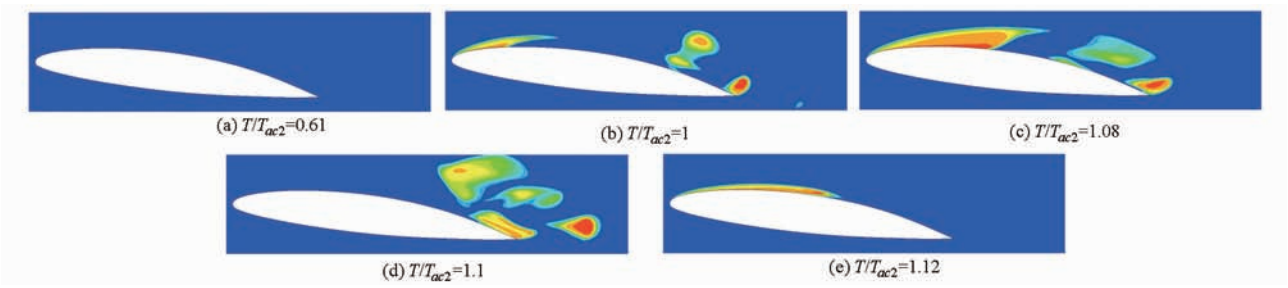

图 7 不同时刻空化发展过程($a_2 = 2.5$ m/s^2)

Fig. 7 Cavitation process at different times

右，在 $T/T_{ac}=1.12$ 左右结束第 1 个周期。

3.3　不同加速度下速度场分布

图 8 分别给出了不同加速流下不同时刻翼型周围速度场分布情况。从中可以发现，DES 模型能够较好地模拟出翼型周围速度场分布和旋涡的变化规律。对比两者可以明显看出小加速流下，翼型尾翼处旋涡发展得更加充分。从图 8a ~ 8c 看出，初始阶段，翼型前缘在主流和回射流的作用下出现小型旋涡，而尾部在强烈的回射流作用下，产生大型的顺时针方向的旋涡。并且随着时间的推移，翼型前缘处旋涡消失，尾翼处旋涡增强，同时在主流推动下向翼型后方移动直至消失。

3.4　不同加速度下翼型升阻力特性

从图 9 中可以发现，在 2 种不同加速度下翼型升力系数的变化趋势是一致的，开始先从一个较大的值快速下降到较小值，然后平稳过渡到 T_{ac}，并且在该点左右达到了极大值，随后呈周期性振荡走势来回波动。第 1 种加速流下升力系数振荡范围在 −0.18 ~ 1.42 之间，第 2 种振荡范围在 −0.05 ~ 1.4 之间。加速度越大，升力振荡范围越大。

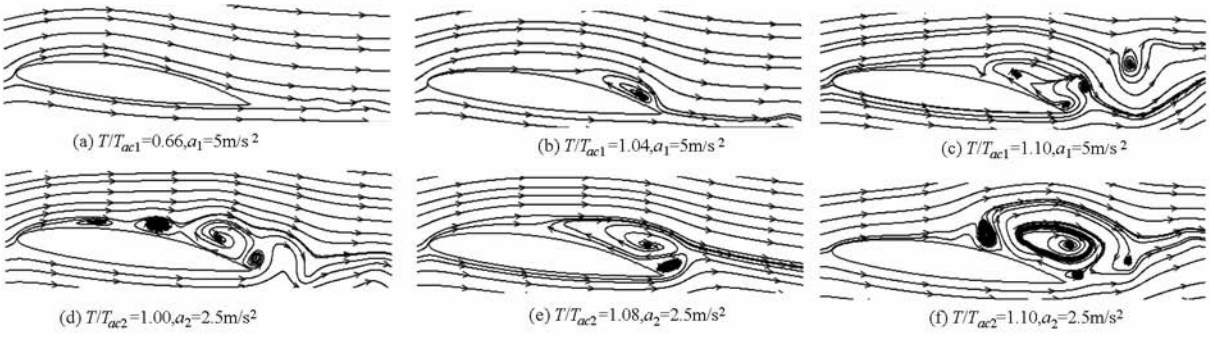

图 8　不同时刻速度场分布

Fig. 8　Velocity field at different times

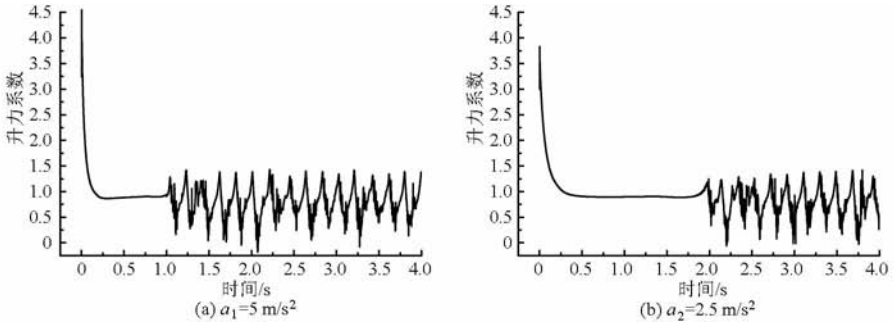

图 9　不同时刻升力系数

Fig. 9　Lift coefficient at different time

从图 10 可以看出，在 2 种不同加速度下翼型阻力系数的变化趋势是一致的，开始先从一个较大的值快速下降到较小值，然后平稳过渡到 T_{ac}，并且在该点左右达到了极大值，随后呈周期性振荡走势来回波动。第 1 种加速流下阻力系数振荡范围在 −0.04 ~ 0.3 之间，第 2 种阻力系数振荡范围在 −0.08 ~ 0.3 之间。加速度越大，阻力振荡范围越小。

3.5　不同加速度下空泡体积分数对比

图 11 为不同加速流下，不同时刻翼型表面空泡总体积分数，该体积分数变化与 3.1 节中空化发展趋势相同，当 $a_1=5\ \mathrm{m/s^2}$ 时，$T=0.66$ s 时空泡体积

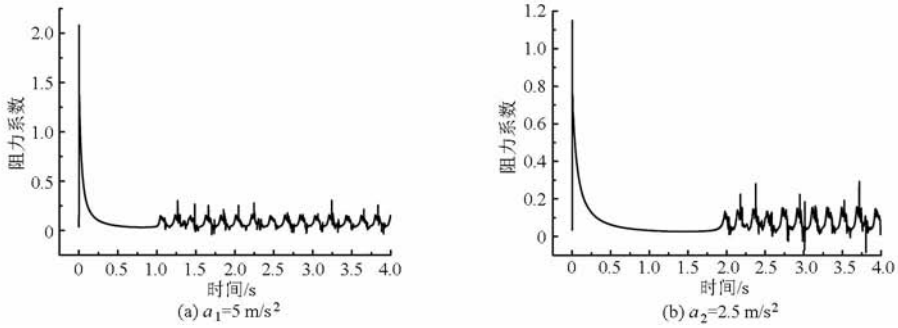

图 10　不同时刻阻力系数

Fig. 10　Drag coefficient at different time

分数开始增加,$T=1.08$ s 时达到极大值,所需时间 0.42 s,往后成不规律周期性变化。当 $a_2=2.5$ m/s^2 时,$T=1.22$ s 时空泡体积分数开始增加,$T=2.23$ s 时达到极大值,所需时间为 1.01 s。对比两者可以发现,在低加速度情况下,空泡体积分数从零到极大值所需时间更长,发展过程更加缓慢。

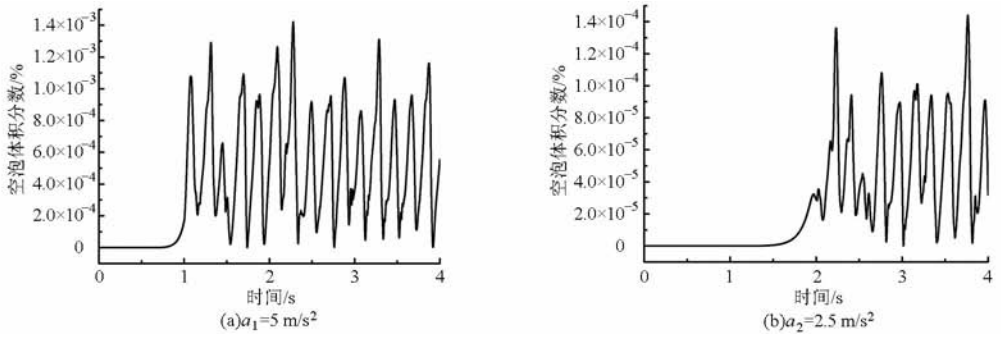

图 11 不同时刻空泡体积分数

Fig. 11 Vapor volume fraction at different time

4 结论

(1)通过模拟与实验对比,验证了分离涡湍流模型(DES)和 Zwart 空化模型可以较好地预测绕水翼加速流下空化情况。并且能够为后续水力机械启动加速过程的空化特性研究提供参考依据。

(2)在加速启动过程中,空泡首先在翼型的前缘产生,经过一段时间后发展壮大,然后在翼型尾翼处分离,前缘处空泡减少,尾翼处空泡增加并向后衍生,直至破裂。并且在随后的过程中反复呈现这种规律。不同加速情况下,空化都首先产生于总加速时间的 0.6 倍左右,在总加速时间的 1.12 倍左右结束第 1 个周期。

(3)加速度越小,翼型尾翼处旋涡发展得越充分。翼型前缘小型旋涡是由主流和回射流的作用产生的,而尾翼大型的顺时针方向旋涡是由强烈的回射流作用而产生的。同时随着时间的推移,翼型前缘处旋涡消失,尾翼处旋涡增强。

(4)不同加速度下翼型升、阻力系数的变化趋势是一致的,开始先从一个较大的值快速下降到较小值,然后平稳过渡到 T_{ac},并且在该点左右达到了极大值,随后成周期性振荡走势来回波动。加速度越大,升力振荡范围越大,阻力振荡范围越小。

(5)加速度越小,空化发生过程越缓慢,空泡体积分数从零到极大值所需要的时间更长。

参 考 文 献

1 SORIA J, NEW H,T, LIM T T, et al. Multigrid CCDPIV measurements of accelerated flow past an airfoil at an angle of attack of 30°[J]. Experimental Thermal and Fluid Science,2002,27(5):667 - 676.

2 FREYMUTH P. The vortex patterns of dynamic separation: a parametric and comparative study[J]. Progress in Aerospace Sciences, 1985, 22(3):161 - 208.

3 HUTTON S P. Studies of cavitation erosion and its relation to cavitating flow patterns[C]// Proceedings of the International Symposium on Cavitation, 1986, 1: 21 - 29.

4 KUBOTA A, KATO H, YAMAGUCHI H, et al. Unsteady structure measurement of cloud cavitation on a foil section using conditional sampling technique[J]. ASME Journal of Fluids Engineering, 1989, 111(2): 204 - 210.

5 SPALART P R, JOU W H, STRELETS M, et al. Comments on the feasibility of LES for wings, and on a hybrid RANS/LES approach[C]// LIU C, LIU Z. Advances in DNS/LES, 1st AFOSR International Conference on DNS/LES. Columbus: Greyden Press,1997: 137 - 148.

6 FORSYTHE J R, MITCHELL A, HAJEK D. DES and RANS simulations of delta wing vortical flows[M]. Colorado Springs: American Institute of Aeronautics and Astronautics, 2002.

7 吴大转,焦磊,王乐勤.绕翼型加速流动的数值模拟-加速度的影响[J].工程热物理学报,2006,27(3):423 - 425.
WU Dazhuan, JIAO Lei, WANG Leqin. Numerical simulation of accelerated flow past an airfoil: influence of acceleration[J]. Journal of Engineering Thermophysics, 2006,27(3):423 - 425. (in Chinese)

8 郝宗睿,王乐勤,吴大转,等. 水翼瞬态启动非定常流动数值模拟[J]. 大连海事大学学报,2009,35(2):131 - 135,144.
HAO Zongrui, WANG Leqin, WU Dazhuan, et al. Numerical simulation of unsteady flow of impulsively started hydrofoil[J]. Journal of Dalian Maritime University, 2009, 35(2):131 - 135,144. (in Chinese)

9 郝宗睿,王乐勤,吴大转. 水翼非定常空化流场的数值模拟[J]. 浙江大学学报:工学版,2010,44(5):1043 - 1048.
HAO Zongrui, WANG Leqin, WU Dazhuan. Numerical simulation of unsteady cavitating flow on hydrofoil[J]. Journal of Zhejiang

University: Engineering Science, 2010, 44(5): 1043 - 1048. (in Chinese)

10 黄彪,王国玉. 基于 $k-\omega$ SST 模型的 DES 方法在空化流动计算中的应用[J]. 中国机械工程,2010,21(1):85 - 89.
HUANG Biao, WANG Guoyu. Application of a SST - DES turbulence model for computation of cavitating flows[J]. China Mechanical Engineering, 2010, 21(1):85 - 89. (in Chinese)

11 李栋,Igor Menshov,中村佳朗. 翼型失速特性的 RANS 方法与 DES 方法数值模拟对比分析[J]. 西北工业大学学报,2006,24(2):228 - 231.
LI Dong, IGOR Menshov, Yoshiaki Nakamura. Is DES approach better than RANS approach for airfoil stall simulation? [J]. Journal of Northwestern Polytechnical University, 2006, 24(2):228 - 231. (in Chinese)

12 HUITENGA H, MITRA N. Improving startup behavior of fluid couplings through modification of runner geometry: part I - fluid flow analysis and proposed improvement[J]. ASME Journal of Fluids Engineering, 2000, 122(4):683 - 688.

13 HUITENGA H, MITRA N. Improving startup behavior of fluid couplings through modification of runner geometry: part II - modification of runner geometry and its effects on the operation characteristics[J]. ASME Journal of Fluids Engineering, 2000, 122(4):689 - 693.

14 刘竹青,朱强,杨魏,等. 双吸离心泵关阀启动过程的瞬态特性研究[J]. 农业机械学报,2015,46(10):44 - 48,55.
LIU Zhuqing, ZHU Qiang, YANG Wei, et al. Transient characteristics of double-suction centrifugal pump during starting period under shut-off condition[J]. Transactions of the Chinese Society for Agricultural Machinery, 2015, 46(10): 44 - 48, 55. (in Chinese)

15 LEROUX J B, COUTIER-DELGOSHA O, ASTOLFI J A. A joint experimental and numerical study of mechanisms associated to instability of partial cavitation on two-dimensional hydrofoil[J]. Physics of Fluids, 2005, 17(5):052101.

16 LEROUX J B, ASTOLFI J A, BILLARD J Y. An experimental study of unsteady partial cavitation[J]. ASME Journal of Fluids Engineering, 2004, 126(1):94 - 101.

17 ZWART P J, GERBER A G, BELAMRI T. A two-phase flow model for predicting cavitation dynamics[C]// Fifth International Conference on Multiphase Flow, Yokohama, Japan, 2004: 152.

18 HUANG B, WANG G, ZHAO Y, et al. Physical and numerical investigation on transient cavitating flows[J]. Science China Technological Sciences, 2013,56(9):2207 - 2218.

19 HUANG B, YOUNG Y L, WANG G, et al. Combined experimental and computational investigation of unsteady structure of sheet/cloud cavitation[J]. Journal of Fluids Engineering, 2013,135(7):071301.

20 HUANG B, ZHAO Y, WANG G. Large eddy simulation of turbulent vortex-cavitation interactions in transient sheet/cloud cavitating flows[J]. Computers & Fluids, 2014,92:113 - 124.